Journal of Alloys and Compounds 489 (2010) 678–684

Contents lists available at ScienceDirect

Journal of Alloys and Compounds

journal homepage: www.elsevier.com/locate/jallcom

Investigation of small Sn–3.5Ag–0.5Cu additions on the microstructure and properties of Sn–8Zn–3Bi solder on Au/Ni/Cu pads

Asit Kumar Gain[a], Tama Fouzder[b], Y.C. Chan[a,*], Ahmed Sharif[c], Winco K.C. Yung[d]

[a] Department of Electronic Engineering, City University of Hong Kong, Tat Chee Avenue, Kowloon Tong, Hong Kong
[b] Electronic and Telecommunication Engineering, Department, University of Development Alternative, Dhaka, Bangladesh
[c] Department of Materials and Metallurgical Engineering, Bangladesh University of Engineering and Technology (BUET), Dhaka, Bangladesh
[d] Department of Industrial and Systems Engineering, The Hong Kong Polytechnic University, Hung Hom, Kowloon, Hong Kong

ARTICLE INFO

Article history:
Received 1 September 2008
Accepted 23 September 2009
Available online 2 October 2009

Keywords:
Multiple reflows
Pb-free
Ball grid array solder joints
Shearing strength
Microstructure

ABSTRACT

The formation of intermetallic compounds and the shear strength of Sn–Zn–Bi solder alloys with various (0, 1, 3, 5 and 7 wt%) weight percentages of Sn–Ag–Cu were investigated on Au/Ni metallized Cu pads depending on the number of reflow cycles. In Sn–Zn–Bi solder joints, scallop-shaped $AuZn_3$ intermetallic compound (IMC) particles were found at the interfaces and in the solder ball regions, fine Bi- and needle-shaped Zn-rich phase were observed in the Sn matrix. After Sn–Ag–Cu additions, an additional Ag–Zn intermetallic compound layer was adhered to the top surface of the $AuZn_3$ layer at the interface and fine spherical-shaped $AgZn_3$ intermetallic compound particles were detected in the solder ball regions together with Bi- and Zn-rich phase volumes. After the addition of Sn–Ag–Cu, the shear strength of Sn–Zn–Bi solder joints increased due to the formation of the fine $AgZn_3$ intermetallic compound particles. The shear strengths of Sn–Zn–Bi and Sn–Zn–Bi/7 wt% Sn–Ag–Cu solder joints after one reflow cycle were about 44.5 and 53.1 MPa, respectively and their shear strengths after eight reflow cycles were about 43.4 and 51.6 MPa, respectively.

1. Introduction

The development of environmental-friendly solders, namely, lead-free solders, has become a great concern for material scientists in recent years since lead is a toxic element and is harmful to health [1–5]. Nowadays, various types of Sn-based, lead-free solders, such as Sn–Zn, Sn–Ag, Sn–Ag–Cu and Sn–Cu etc., have been developed to replace the conventional Sn–Pb eutectic solder traditionally used in the electronic packaging industry [6,7]. Up to now, to fulfill some requirements in certain special applications, the development of new candidate solders has continued. Since one role of the solder alloys is to serve as a structural material to connect the components, one of the major concerns in the development of electronic packaging is the reliability of the solder joints [8].

Among the lead-free solders, eutectic or near eutectic Sn–Zn solder is regarded as a suitable replacement for Sn–Pb solders due to its low melting temperature as compared with other Sn-based, lead-free solder as well as low cost [9]. However, Sn–Zn eutectic solder is difficult to handle practically due to its highly active characteristics that lead to poor wettability, easy oxidation and micro-void formation [10–11]. These deficiencies have to be resolved to increase the practical applications of this solder alloy. Shih and Lin [12] and Shohji et al. [13] reported that the addition of Bi in near eutectic Sn–Zn solders improved the soldering properties such as giving high joint strength, good wettability and low melting temperature, in electronic packaging. However, the addition of Bi into the Sn–Zn eutectic alloy formed on a Cu substrate was also found to result in poor oxidation resistance and joint degradation under exposure to high thermal and humidity conditions [14,15]. It is well known that the poor oxidation resistance of Sn–Zn alloy is due to the oxidation of Zn. In general, water vapor and oxygen diffuse into alloys along the grain boundaries and correspondingly Zn diffuses to the grain boundaries forming ZnO. If the amount of Zn phase in the Sn–Zn eutectic alloy can be reduced or fixed by forming IMC particles or block the diffusion of water vapor and oxygen along grain boundaries by the addition of IMC particles, it is expected that the oxidation resistance can be improved.

One innovative, potentially viable and economically affordable approach, to stabilize a fine grain microstructure, give homogeneous deformation of solder joints as well as improve the mechanical properties of a solder, is the addition of an appropriate secondary phase to a solder matrix for the formation of Zn-based intermetallic compound. In this study, as a new approach, Sn–Zn–Bi alloys with various additions of secondary Sn–3.5Ag–0.5Cu were prepared by mechanically dispersing different weight percentages (0, 1, 3, 5 and 7 wt%) of Sn–Ag–Cu powder into Sn–Zn–Bi solder

* Corresponding author. Tel.: +852 27887130; fax: +852 27888044.
E-mail address: eeycchan@cityu.edu.hk (Y.C. Chan).

0925-8388/$ – see front matter © 2009 Elsevier B.V. All rights reserved.
doi:10.1016/j.jallcom.2009.09.150

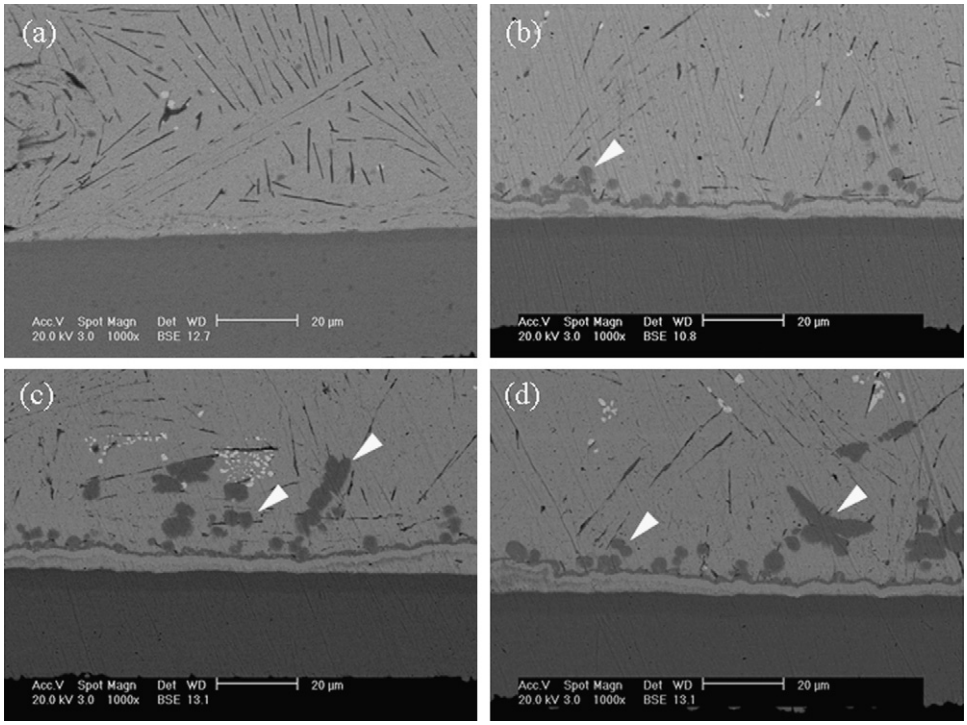

Fig. 1. SEM micrographs of cross-sections of (a) Sn–Zn–Bi, (b) Sn–Zn–Bi/3 wt% Sn–Ag–Cu, (c) Sn–Zn–Bi/5 wt% Sn–Ag–Cu and (d) Sn–Zn–Bi/7 wt% Sn–Ag–Cu solder joints after one reflow cycle.

paste. The main purpose of this study is to investigate the correlation of interfacial microstructure and shear strengths of Sn–Zn–Bi solder with various additions of Sn–Ag–Cu as a function of the number of reflow cycles. In addition, the distribution of intermetallic compound particles is systematically investigated again as a function of the number of reflow cycles.

2. Experimental procedure

The Sn–8Zn–3Bi solders balls with different weight percentages of Sn–3.5Ag–0.5Cu were prepared primarily by mechanically dispersing different weight percentages (1, 3, 5, and 7 wt%) of Sn–3.5Ag–0.5Cu (Shenzhen Junye Nano Material Co., China) micro-powder into a Sn–8Zn–3Bi paste. The mixture was blended manually for at least 30 min to ensure a uniform distribution of the Sn–Ag–Cu particles. Then, the paste mixture was printed on to alumina substrates using a stainless steel stencil with a thickness of 0.15 mm and reflowed in a reflow oven (BTU VIP-70N) at 245 °C to prepare 0.76 mm diameter solder balls.

The solder joints were made by soldering between flexible ball grid array (BGA) substrates with Au/Ni/Cu coated pads. The solder balls were placed on the pre-fluxed coated pad and then reflow at 245 °C in a reflow oven (BTU VIP-70N) with a belt speed 10 cm min^{-1}. After the reflow process, the samples were cooled to room temperature. Then, each BGA solder joint was cleaned with isopropyl alcohol (IPA). These samples were prepared for observation of the IMC particle distribution

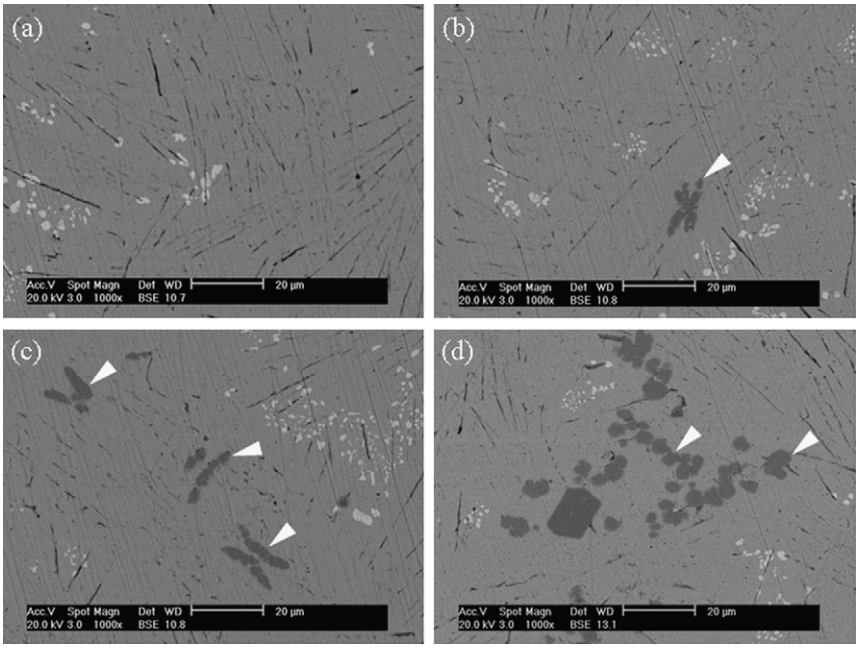

Fig. 2. SEM micrographs of (a) Sn–Zn–Bi, (b) Sn–Zn–Bi/1 wt% Sn–Ag–Cu, (c) Sn–Zn–Bi/3 wt% Sn–Ag–Cu and (d) Sn–Zn–Bi/7 wt% Sn–Ag–Cu solder joints after one reflow cycle.

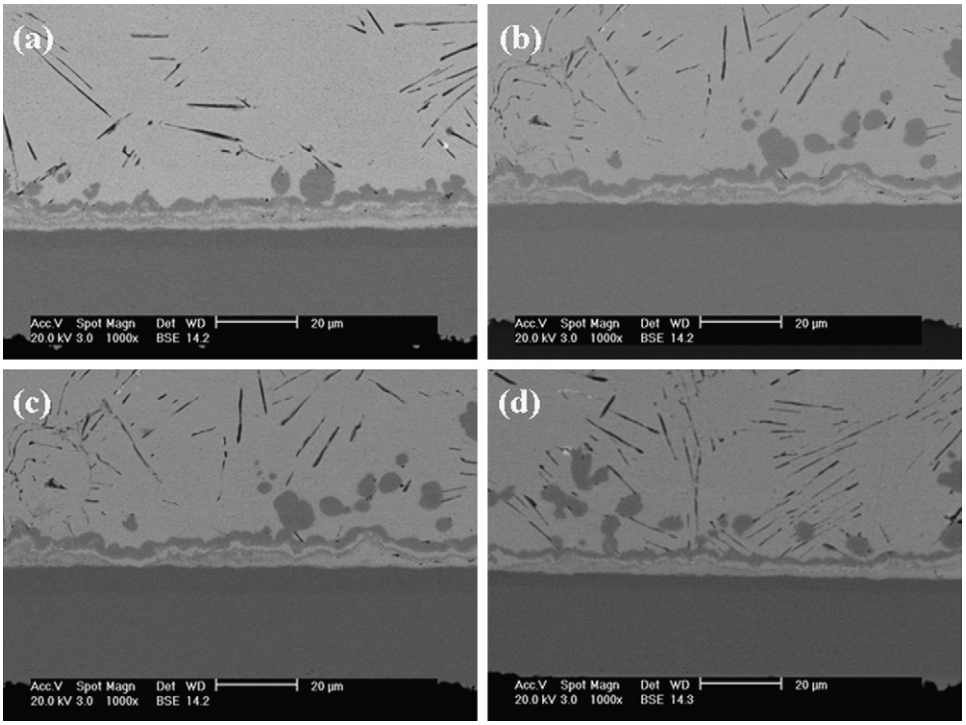

Fig. 3. SEM micrographs of (a) Sn–Zn–Bi/1 wt% Sn–Ag–Cu, (b) Sn–Zn–Bi/3 wt% Sn–Ag–Cu, (c) Sn–Zn–Bi/5 wt% Sn–Ag–Cu and (d) Sn–Zn–Bi/7 wt% Sn–Ag–Cu solder joints after four reflow cycles.

formed at the interface on both the cross-sections and top surfaces using standard metallographic procedures. The reflow specimens were mounted in resin, then mechanically ground by different grit size emery papers and polished with 0.5 μm Al_2O_3 powder. A scanning electron microscope (SEM, Philips XL 40 FEG) employing with the backscattered electron (BSE) imaging mode was used for the observation of microstructures. Additionally, an energy diffraction spectrometer (EDAX International, model no. DX-4) was adopted to determine phase compositions. The accuracy of the compositional measurements was typically ±5%. To find out the formula composition of the intermetallic compound (IMC) particles, the chemical analyses of the EDX spectra were corrected by standard atomic number, absorption, fluorescence (ZAF) software. Before the SEM observations, the samples were sputter coated with Au to avoid any effects due to charging.

Ball shear tests were performed on the reflowed samples using a shear tester (PTR-1000, Rhesca Co. Ltd., Japan) with a shear tool height of 50 μm and shear speed

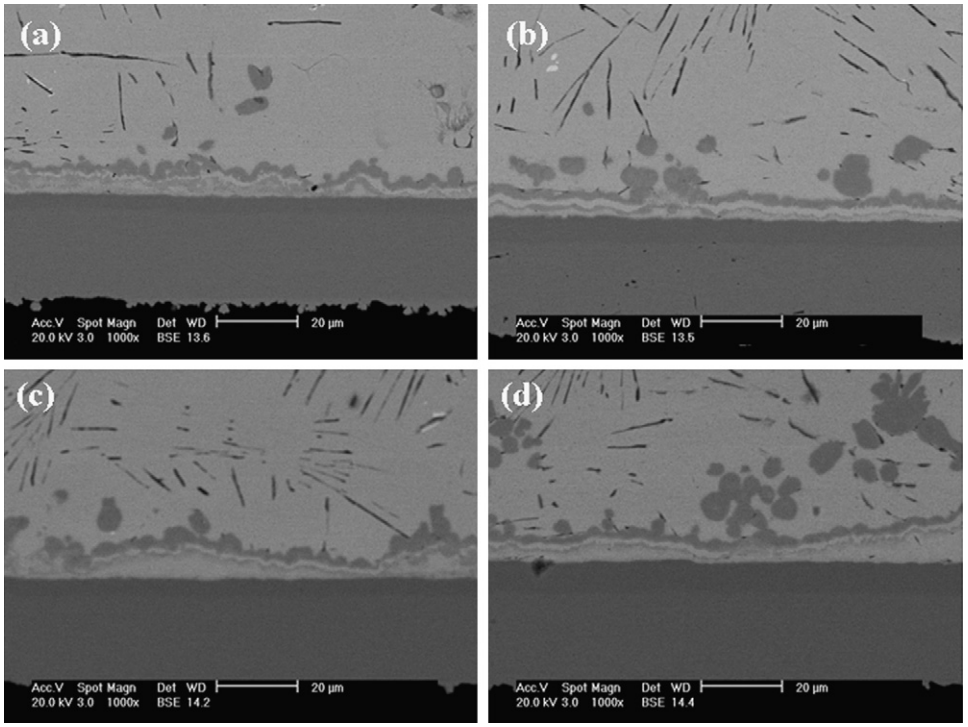

Fig. 4. SEM micrographs of (a) Sn–Zn–Bi/1 wt% Sn–Ag–Cu, (b) Sn–Zn–Bi/3 wt% Sn–Ag–Cu, (c) Sn–Zn–Bi/5 wt% Sn–Ag–Cu and (d) Sn–Zn–Bi/7 wt% Sn–Ag–Cu solder joints after eight reflow cycles.

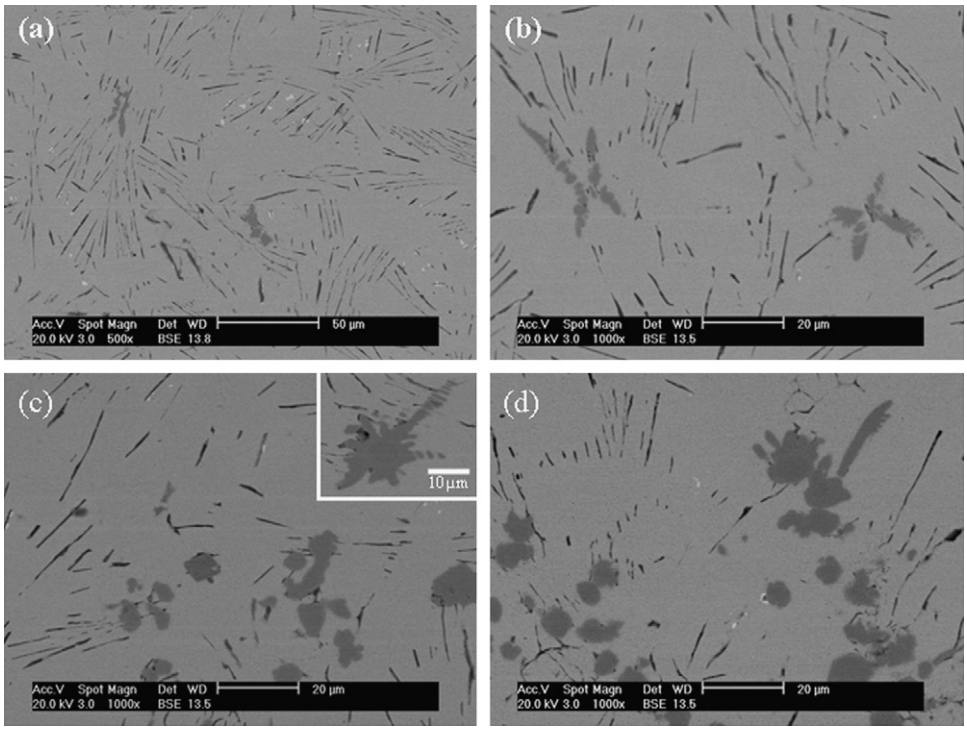

Fig. 5. SEM micrographs of (a) Sn–Zn–Bi/1 wt% Sn–Ag–Cu, (b) Sn–Zn–Bi/3 wt% Sn–Ag–Cu, (c) Sn–Zn–Bi/5 wt% Sn–Ag–Cu and (d) Sn–Zn–Bi/7 wt% Sn–Ag–Cu solder joints after eight reflow cycles.

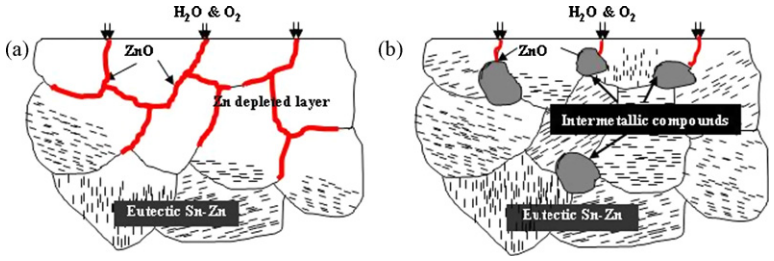

Fig. 6. Schematic diagrams of the oxidation of Sn–Zn–Bi alloys. (a) ZnO formed on the Sn grain boundaries near the free surface causes cracks and (b) formation of intermetallic compounds on the grain boundaries.

of 550 μm/s. The average strength of twenty solder balls with the minimum and maximum values removed was recorded for each condition. After ball shear testing, the fracture surfaces and compositions were investigated thoroughly using SEM and EDX techniques.

3. Results and discussion

Fig. 1 shows cross-sectional backscattered electron micrographs of interfaces between (a) Sn–Zn–Bi, (b) Sn–Zn–Bi/3 wt% Sn–Ag–Cu, (c) Sn–Zn–Bi/5 wt% Sn–Ag–Cu, and (d) Sn–Zn–Bi/7 wt% Sn–Ag–Cu and Au/Ni metallized Cu pads after one reflow cycle. In the Sn–Zn–Bi solder, the scallop-shaped $AuZn_3$ intermetallic compound layer was found at the interfaces. However, after the addition of Sn–Ag–Cu, an additional Ag–Zn intermetallic compound layer in dark contrast was observed at the top surface of the $AuZn_3$ intermetallic compound layer. In addition, fine spherical-shaped $AgZn_3$ intermetallic compound particles in dark contrast were detected near the Ag–Zn intermetallic compound layer as indicated with arrow heads in Fig. 1(b–d). Also, the amount of $AgZn_3$ intermetallic compound particles increased with an increase in the Sn–Ag–Cu content.

Fig. 2 shows backscattered electron micrographs of Sn–Zn–Bi solder joints as a function of the Sn–Ag–Cu content of (a) 0 wt%,

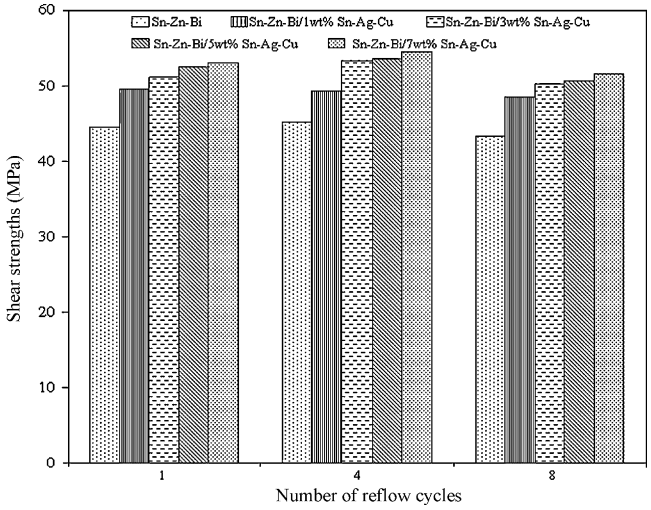

Fig. 7. Shear strengths of Sn–Zn–Bi solder joints with various additions of Sn–Ag–Cu as a function of the number of reflow cycles.

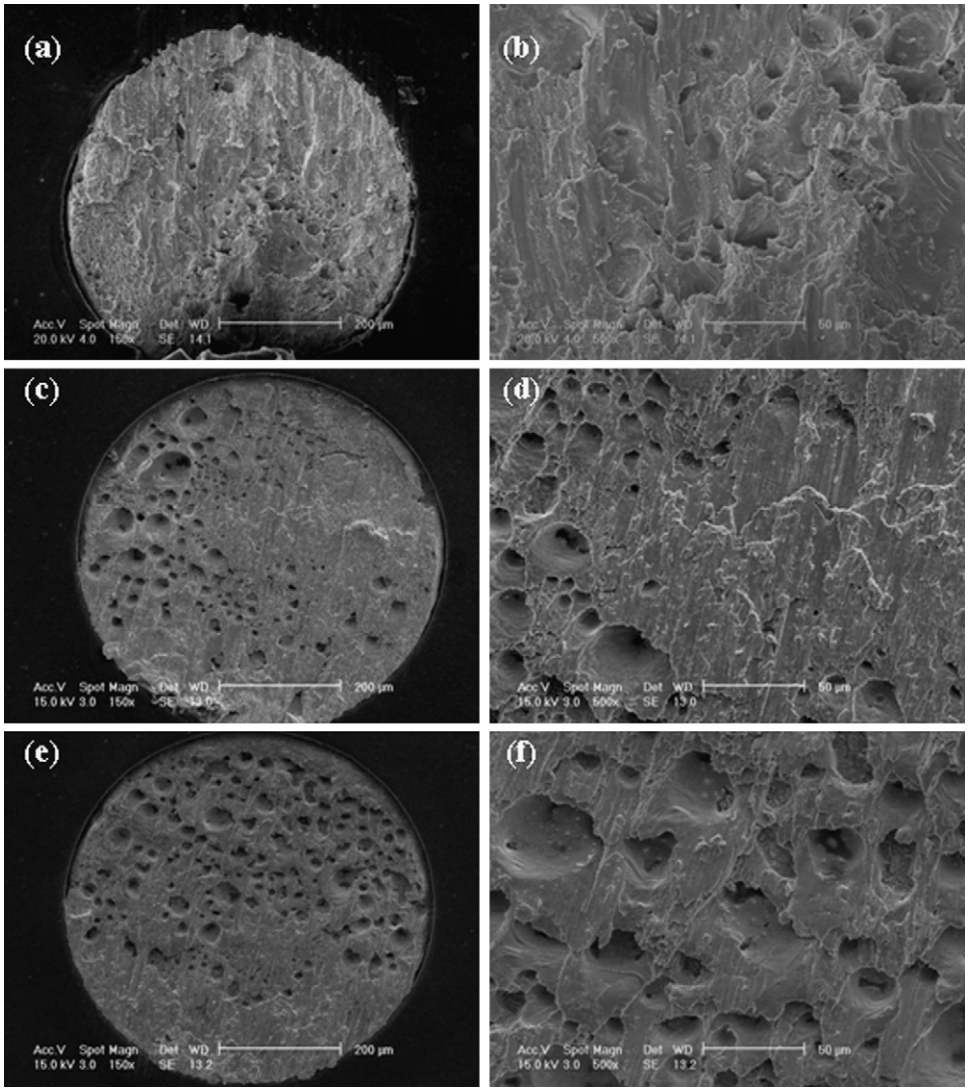

Fig. 8. SEM fracture surfaces of (a and b) Sn–Zn–Bi, (c and d) Sn–Zn–Bi/3 wt% Sn–Ag–Cu and (e and f) Sn–Zn–Bi/7 wt% Sn–Ag–Cu solder joints after one reflow cycle.

(b) 3 wt%, (c) 5 wt% and (d) 7 wt%, which were taken from solder ball regions after one reflow cycle. In the Sn–Zn–Bi solder joint shown in Fig. 2(a), fine Bi-rich particles in bright contrast as well as a needle-shaped Zn-rich phase were found in the Sn matrix. However, after the addition of Sn–Ag–Cu, fine spherical-shaped $AgZn_3$ intermetallic compound particles in dark contrast were found as well as Bi-rich and needle-shaped Zn-rich phases in the Sn matrix as shown in Fig. 2(b–d). The amount of $AgZn_3$ intermetallic compound particles increased with an increase in the Sn–Ag–Cu content.

Fig. 3 shows cross-sectional backscattered electron micrographs of interfaces between Sn–Zn–Bi solder joints with various additions of Sn–Ag–Cu of (a) 1 wt%, (b) 3 wt%, (c) 5 wt%, (d) 7 wt% and Au/Ni metallized Cu pads after four reflow cycles. After four reflow cycles, at the interfaces, a layer type structure was observed which consisted of $AuZn_3$ intermetallic compound in bright contrast and Ag–Zn intermetallic compound in dark contrast. However, with an increase in the number of reflow cycles the layer thickness and the size of the $AgZn_3$ intermetallic compound particles increased as compared with the case after one reflow cycle.

Fig. 4 shows cross-sectional backscattered electron micrographs of Sn–Zn–Bi solder joints with various additions of Sn–Ag–Cu of (a) 1 wt%, (b) 3 wt%, (c) 5 wt% and (d) 7 wt% after eight reflow cycles. After eight reflow cycles, at the interfaces the $AuZn_3$ and Ag–Zn intermetallic compound layer thicknesses were not significantly change as compared with that seen in solder joints after four reflow cycles as shown in Fig. 3. However, the size of the individual distributed $AgZn_3$ intermetallic compound particles had increased after eight reflow cycles.

Fig. 5 shows cross-sectional backscattered electron micrographs of Sn–Zn–Bi solder with various additions of Sn–Ag–Cu of (a) 1 wt%, (b) 3 wt%, (c) 5 wt% and (d) 7 wt% after eight reflow cycles. In the Sn–Ag–Cu containing solder joints, fine Bi-rich, needle-shaped Zn-rich phases as well as $AgZn_3$ intermetallic compound particles were found in the Sn matrix. In addition, with an increase in the number of reflow cycles the $AgZn_3$ intermetallic compound particle size increased due to an increase in the reaction time between Zn and Ag. However, after eight reflow cycles, some $AgZn_3$ intermetallic compound appeared with a sunflower-shaped structure as shown in the enlarged image in Fig. 5(c). On the other hand, with an increase in the Sn–Ag–Cu content, the amount of needle-shaped Zn-rich phase was significantly decreased as shown in Fig. 5(a–d). This decrease of the Zn-rich phase will be expected to improve the oxidation resistance of joints during reliability tests.

With an exposure of Sn–Zn–Bi solder to a high-temperature and high-humidity atmosphere, the Zn on the free surface will soon react with water vapor or oxygen and form ZnO on the free surface. At the same time, Zn will also diffuse along the Sn grain boundaries to the free surface and form oxides near the free surface because

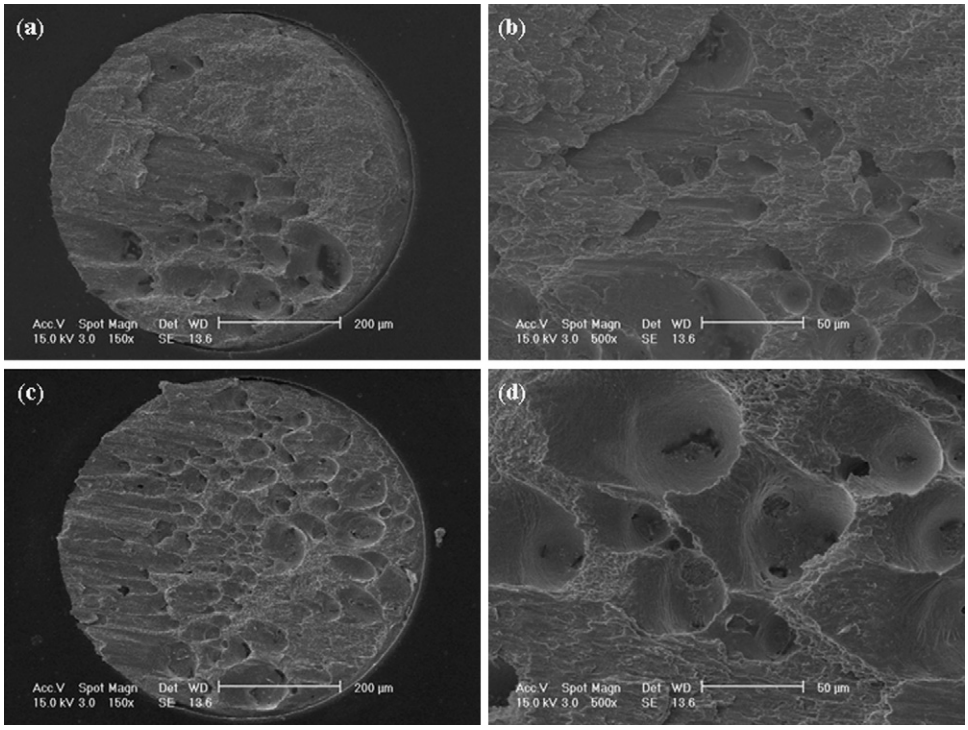

Fig. 9. SEM fracture surfaces of (a and b) Sn–Zn–Bi/1 wt% Sn–Ag–Cu and (c and d) Sn–Zn–Bi/7 wt% Sn–Ag–Cu solder joints after eight reflow cycles.

of its rapid diffusion along the Sn grain boundaries [16]. During the reaction of Zn to form ZnO, the stress induced by the volume expansion in forming ZnO, especially along the Sn grain boundaries, increases which may cause cracks along these boundaries. As a result, there is a serious degradation of the joint strength for Sn–Zn–Bi alloys due to the formation of ZnO oxide at grain boundaries as shown schematically in Fig. 6(a). To minimize the formation of cracks as well as to improve the oxidation resistance of the Sn-based solder alloy, Sn–Ag–Cu powder was added to aid the formation of intermetallic compounds in the grain boundaries. In the present study, the formation of spherical-shaped $AgZn_3$ intermetallic compound particles can improve the oxidation resistance of the Sn–Zn–Bi solder. During soldering, these intermetallic compounds will form in the grain boundaries and later on block the penetration of water vapor and oxygen which in turn reduces the formation of ZnO along the grain boundaries as shown in Fig. 6(b).

Since solder joints are often subjected to mechanical loading during processing and system use, good mechanical properties of solder joints, such as high shear strength and creep resistance, are essential for solder joint reliability. Therefore, ball shear tests were performed to evaluate the strength of solder joints as a function of the number of reflow cycles. Fig. 7 shows the variation of ball shear strength of Sn–Zn–Bi solder joints as a function of Sn–Ag–Cu content and the number of reflow cycles. From this bar diagram, it is clear that the shear strengths of the Sn–Ag–Cu containing solder joints did not change much as a function of the number of reflow cycles. However, the solder joints with a high percentage of Sn–Ag–Cu showed a consistently higher strength than that of solder joints with a lower of Sn–Ag–Cu content at different numbers of reflow cycles. It is reasonable to suggest that the strength of

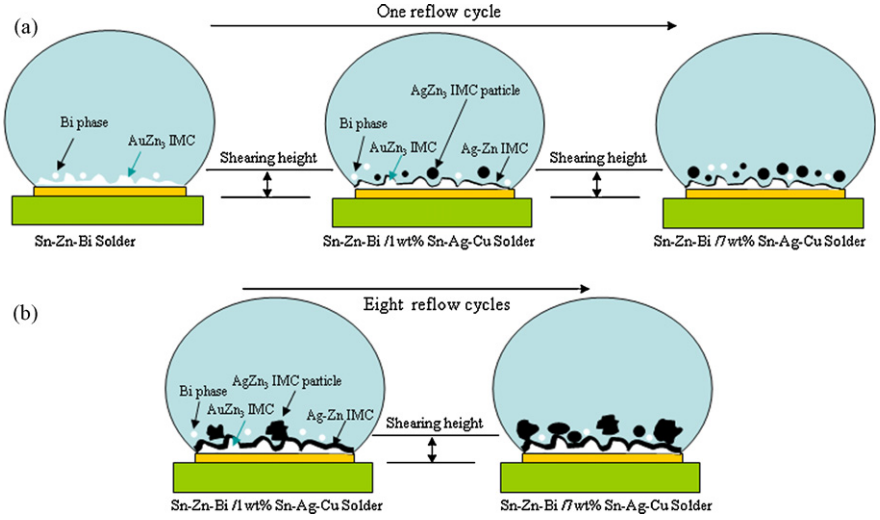

Fig. 10. Schematic diagram of BGA solder joints of (a) after one reflow cycle and (b) after eight reflow cycles.

the bulk solder was enhanced by the addition of Sn–Ag–Cu because the solder matrix had a high content of $AgZn_3$ intermetallic compound particles giving dispersion strengthening. From this result, we suggest that the thickness and morphology of the interfacial intermetallic compound layer did not play a critical role in controlling the shear strength of solder joints with different Sn–Ag–Cu additions. The shear strengths of Sn–Zn–Bi solder joints without Sn–Ag–Cu additions after one reflow cycle and eight reflow cycles were about 44.5 and 43.4 MPa, respectively. However, the shear strengths of Sn–Zn–Bi/7 wt% Sn–Ag–Cu solder joints after one reflow cycle and eight reflow cycles were about 53.1 and 51.6 MPa, respectively.

After measuring the interfacial strength, fracture surfaces of the solder were examined using a scanning electron microscope. Fig. 8 shows the SEM images of fracture surfaces of Sn–Zn–Bi solder joints depending on the Sn–Ag–Cu content of (a and b) 0 wt%, (c and d) 3 wt% and (e and f) 7 wt% after one reflow cycle. In the Sn–8Zn–3Bi solder joint without Sn–Ag–Cu additions, the fracture mode showed semi ductile behavior as seen in Fig. 8(a and b). However, typical ductile fractures with a very rough dimpled surface were found after the additions of Sn–Ag–Cu as shown in Fig. 8(c–f). In addition, the roughness of the fracture surfaces increased with an increase in the Sn–Ag–Cu additions due to the formation of large $AgZn_3$ intermetallic compound particles.

Fig. 9 shows SEM fracture surfaces of Sn–Zn–Bi solder joints with different Sn–Ag–Cu contents of (a and b) 3 wt% and (e and f) 7 wt% after eight reflow cycles. From these SEM micrographs, it is clear that the fracture mode seen is a typical ductile fracture with very rough dimpled surfaces the same as in Fig. 8(c–f). However, the dimple size increased with an increase in the number of reflow cycles due to the increase in the size of the $AgZn_3$ intermetallic compound particles.

Since the fracture occurred inside the solder, the difference in shear strength should be independent of the interfacial structure. After the addition of Sn–Ag–Cu, the shear strengths consistently increased with an increase in the Sn–Ag–Cu content as a result of the uniform distribution of fine $AgZn_3$ intermetallic compound particles. In addition, the solder joints with a higher percentage of Sn–Ag–Cu showed a higher strength than that of solder joints with a lower Sn–Ag–Cu content at different numbers of reflow cycles due to the strengthening effect of $AgZn_3$ intermetallic compound particles. It was also found that after eight reflow cycles, the shear strengths of Sn–Ag–Cu containing solder joints were slightly decreased due to the agglomeration of $AgZn_3$ intermetallic compound particles as shown schematically in Fig. 10.

4. Conclusions

In the present study, the interfacial reactions, the morphology of intermetallic compound particles and shear strength between Sn–Zn–Bi solder joints with different weight percentages of Sn–Ag–Cu and Au/Ni metallized Cu substrates were investigated for up to eight reflow cycles. The results of this study are summarized as follows:

1. At the interfaces between the solder and Au/Ni metallized Cu pads, scallop-shaped $AuZn_3$ intermetallic compound particles were found in Sn–Zn–Bi solder joints. However, after the addition of Sn–Ag–Cu, an additional Ag–Zn intermetallic compound layer was observed at the top surface of the $AuZn_3$ layer. The intermetallic layer thickness increased with an increase in the number of reflow cycles.
2. In the solder ball regions, a fine Bi-rich and Zn-rich phases were detected in the Sn matrix in the Sn–Zn–Bi solder. However, in the Sn–Ag–Cu containing solder joints, additional $AgZn_3$ intermetallic compound particles were found as well as the fine Bi-rich and Zn-rich phases in the Sn matrix. The $AgZn_3$ intermetallic compound particle size increased with an increase in the number of reflow cycles.
3. The solder joints with a high percentage of Sn–Ag–Cu showed consistently higher strength than that of solder joints with a lower Sn–Ag–Cu content at different reflow cycles due to the formation of $AgZn_3$ intermetallic compound particles. In addition, the Sn–Ag–Cu containing solder joints gave a typical ductile fracture with a very rough dimpled surface.

Acknowledgement

The authors acknowledge the financial support provided by City University of Hong Kong for the project 9041222 CERG grant of Hong Kong Research Grants Council and RGC ref. no. 111307 (development of a nano-activator doped surface modifier for Sn–Zn-based lead-free soldering).

References

[1] M. Abtew, G. Selvaduray, Mater. Sci. Eng. R. 27 (5–6) (2000) 95–141.
[2] P.T. Vianco, J.A. Rejent, J. Electron. Mater. 28 (1999) 1127–1137.
[3] M. Rettenmayr, P. Lambeacht, B. Kempf, M. Graff, Adv. Eng. Mater. 7 (10) (2005) 965–969.
[4] F.J. Wang, Z.S. Yu, K. Qi, J. Alloy. Compd. 438 (2007) 110–115.
[5] I.E. Anderson, J.L. Harringa, J. Electron. Mater. 33 (12) (2004) 1485–1496.
[6] R. Mayappan, A.B. Ismail, Z.A. Ahmad, T. Ariga, L.B. Hussain, Mater. Lett. 60 (2006) 2383–2389.
[7] J.W. Yoon, S.B. Jung, Mater. Sci. Eng. A 452–453 (2007) 46–54.
[8] Z.X. Li, M. Gupta, Adv. Eng. Mater. 7 (11) (2005) 1049–1053.
[9] K.I. Chen, S.C. Cheng, S. Wu, K.L. Lin, J. Alloy Compd. 416 (2006) 98–105.
[10] C.Y. Chou, S.W. Chen, Acta Mater. 54 (2006) 2393–2400.
[11] J. Jiang, J.E. Lee, K.S. Kim, K. Suganum, J. Alloy Compd. 462 (2008) 244–251.
[12] P.C. Shih, K.L. Lin, J. Mater. Res. 20 (2005) 219–229.
[13] I. Shohji, C. Gagg, W.J. Plumbridge, J. Electron. Mater. 33 (2004) 923–927.
[14] K.S. Kim, Y.S. Kim, K. Suganuma, H. Nakajima, J. Jpn. Inst. Electron. Packag. 5 (2002) 666–671.
[15] K.S. Kim, T. Matsuura, K. Suganuma, J. Electron. Mater. 35 (2006) 41–47.
[16] J.E. Lee, K.S. Kim, M. Inoue, J. Jiang, K. Suganuma, J. Alloy Compd. 454 (2008) 310–320.